

The Large Extracellular Loop of Organic Cation Transporter 1 Influences Substrate Affinity and Is Pivotal for Oligomerization^{*S}

Received for publication, August 3, 2011, and in revised form, September 6, 2011. Published, JBC Papers in Press, September 6, 2011, DOI 10.1074/jbc.M111.289330

Thorsten Keller[‡], Brigitte Egenberger[‡], Valentin Gorboulev[‡], Frank Bernhard[§], Zeljko Uzelac[¶], Dmitry Gorbunov[‡], Christophe Wirth^{||}, Stefan Koppatz[‡], Volker Dötsch[§], Carola Hunte^{||**}, Harald H. Sitte[¶], and Hermann Koepsell^{‡1}

From the [‡]Institute of Anatomy and Cell Biology, University of Würzburg, Koellikerstrasse 6, 97070 Würzburg, Germany, the [§]Department of Biophysical Chemistry, University of Frankfurt, 60438 Frankfurt (M), Germany, the [¶]Center of Physiology and Pharmacology, Institute of Pharmacology, Medical University Vienna, 1090 Vienna, Austria, and the ^{||}Institute of Biochemistry and Molecular Biology and the ^{**}BIOSS Centre for Biological Signaling Studies, University of Freiburg, 79104 Freiburg, Germany

Background: Organic cation transporter OCT1 forms oligomers.

Results: The intact structure of the large extracellular loop of OCT1 is pivotal for oligomerization. Oligomerization increases membrane targeting and does not influence substrate affinities.

Conclusion: OCT1 monomers within oligomeric transporter complexes can operate independently, and oligomerization can be changed by extracellular agents.

Significance: The reported data are important to understand transport mechanism and effects of mutations.

Polyspecific organic anion transporters (OATs) and organic cation transporters (OCTs) of the SLC22 transporter family play a pivotal role in absorption, distribution, and excretion of drugs. Polymorphisms in these transporters influence therapeutic effects. On the basis of functional characterizations, homology modeling, and mutagenesis, hypotheses for how OCTs bind and translocate structurally different cations were raised, assuming functionally competent monomers. However, homo-oligomerization has been described for OATs and OCTs. In the present study, evidence is provided that the large extracellular loops (EL) of rat Oct1 (rOct1) and rat Oat1 (rOat1) mediate homo- but not hetero-oligomerization. Replacement of the cysteine residues in the EL of rOct1 by serine residues (rOct1(6ΔC-I)) or breaking disulfide bonds with dithiothreitol prevented oligomerization. rOct1 chimera containing the EL of rOat1 (rOct1(rOat1-I)) showed oligomerization but reduced transporter amount in the plasma membrane. For rOct1(6ΔC-I) and rOct1(rOat1-I), similar K_m values for 1-methyl-4-phenylpyridinium⁺ (MPP⁺) and tetraethylammonium⁺ (TEA⁺) were obtained that were higher compared with rOct1 wild type. The increased K_m of rOct1(rOat1-I) indicates an allosteric effect of EL on the cation binding region. The similar substrate affinity of the oligomerizing and non-oligomerizing loop mutants suggests that oligomerization does not influence transport function. Independent transport function of rOct1 monomers was also demonstrated by showing that K_m values for MPP⁺ and TEA⁺ were not changed after treatment with dithiothreitol and that a tandem protein with two rOct1 monomers showed about 50%

activity with unchanged K_m values for MPP⁺ and TEA⁺ when one monomer was blocked. The data help to understand how OCTs work and how mutations in patients may affect their functions.

Polyspecific organic cation transporters (OCTs)² and organic anion transporters (OATs) of the SLC22 transporter family play a pivotal role in absorption, excretion, and tissue distribution of drugs and various endogenous compounds, such as neurotransmitters and prostaglandins (1, 2). Polymorphisms in OCTs influence the therapeutic effect during treatment of diabetes with metformin and nephrotoxic side effects during treatment of cancer with cisplatin (3). Following the first identifications of rat Oct1 (rOct1) (4) and rat Oat1 (rOat1) (5), functional properties of OCTs and OATs have been studied in detail, and effects of mutations on transport functions have been investigated (1, 2). OCTs and OATs contain 12 transmembrane α -helices (TMHs), intracellular N and C termini, a large extracellular loop between TMH1 and TMH2, and a large intracellular loop between TMH6 and TMH7. Data were obtained that indicate that transporter functions can be regulated by phosphorylation (2, 6). Employing structural models derived from the crystal structures of bacterial transporters of the same superfamily, the major solute facilitator superfamily, mutagenesis attempts have been made to map the substrate binding regions of OCTs and OATs (7–9). Voltage clamp fluorometry and inhibition studies

^{*} This work was supported by Deutsche Forschungsgemeinschaft Grants SFB 487/A4 (to H. K.) and SFB 746/P21 (to C. H.), by the Excellence Initiative of the German Federal and State Governments (EXC 294) (to C. H.), and the Austrian Science Fund/FWF (SFB3506 to H. H. S.).

^S The on-line version of this article (available at <http://www.jbc.org>) contains supplemental Fig. 1.

¹ To whom correspondence should be addressed. Tel.: 49-931-3182700; Fax: 49-931-312087; E-mail: Hermann.Koepsell.de.

² The abbreviations used are: OCT, organic cation transporter; OAT, organic anion transporter; rOct1 and rOct2, rat Oct1 and Oct2, respectively; rOat1, rat Oat1; hOAT1, human OAT1; TMH, transmembrane α -helix; MPP⁺, 1-methyl-4-phenylpyridinium; TEA⁺, tetraethylammonium; MTSET, 2-(trimethylammonium)ethyl methanethiosulfonate bromide; HEK, human embryonic kidney; CFP, cyan fluorescent protein; YFP, yellow fluorescent protein; LMPG, 1-myristoyl-2-hydroxy-*sn*-glycero-3-[phospho-*rac*-(1-glycerol)]; TBuA⁺, tetrabutylammonium; TPeA⁺, tetrapentylammonium; D-PBS, Dulbecco's phosphate-buffered saline; cRNA, complementary RNA.

indicated that OCTs contain high and low affinity cation binding sites that may be accessible from the extracellular side (10). So far, the effects of the mutations have been discussed assuming that OCTs and OATs function as monomers (7–9). To make this assumption a priority is not justified since evidence has been provided that OATs and OCTs form homo-oligomers. Hong and co-workers (11) showed that human OAT1 (hOAT1) forms oligomers in cultured cells and kidney, and we provided evidence that rOat1, rOct1, and rOct2 form homo-oligomers in detergent solution (12). A recent study suggests that the sixth transmembrane α -helix (TMH) of hOAT1 comprises a contact region for oligomerization and that surface expression of hOAT1 was reduced when oligomerization of hOAT1 was disturbed (13).

In the present study, we provide evidence that the structural integrity of the large extracellular loop of rOct1 is critically dependent on disulfide bond formation and that the large extracellular loop is pivotal for homo-oligomerization. We show that mutations within the large extracellular loop may change substrate affinity, but homo-oligomerization has no effect on affinity and transport function.

EXPERIMENTAL PROCEDURES

Materials— ^3H -Labeled 1-methyl-4-phenylpyridinium (MPP^+) (3.1 TBq/mmol) and [^{14}C]TEA $^+$ (1.9 GBq/mmol) were obtained from Biotrend (Köln, Germany). 2-(trimethylammonium)ethyl methanethiosulfonate bromide (MTSET) was purchased from Toronto Research Chemical (Ontario, Canada). All other chemicals were obtained as described earlier (12, 14).

Constructs for Expression in *Xenopus laevis* Oocytes—All mutants were made on the basis of the vector rOct1/pRSSP (15). It contains HindIII and EcoRV sites 5' of rOct1 and a SacI site at the 3'-end of rOct1. Mutants rOct1(rOct2-l) (16), rOct1-FLAG (7), and rOct1(10 Δ C) (17) have been described previously. rOct1(10 Δ C,G478C) was prepared by the overlap extension method of polymerase chain reaction (PCR) (16). Plasmid rOct1(rOat1-l), in which the large extracellular loop of rOct1 is replaced by the corresponding loop of rOat1 (amino acids 40–136), was constructed in analogy to rOct1(rOct2-l) (16). rOct1(rOat1-l)-FLAG and rOct1(6 Δ C-l)-FLAG were obtained by substituting a HindIII/NheI fragment of rOct1-FLAG/pRSSP with the corresponding fragments of rOct1(rOat1-l) or rOct1(6 Δ C-l). To create rOct1(10 Δ C)/rOct1(10 Δ C,G478C) tandem constructs in the pRSSP vector, intermediate constructs were prepared. 1) A new BamHI site was introduced 5' of the nucleotides coding for the first amino acids of the rOct1 mutants, and 2) a short linker containing a BamHI site followed by a SacI site was inserted behind the nucleotides coding for the last amino acids of the rOct1 mutants. BamHI/SacI fragments were isolated from the 5' BamHI constructs and inserted into BamHI/SacI sites of the 3' BamHI/SacI vectors, resulting in the tandem constructs rOct1(10 Δ C)-rOct1(10 Δ C), rOct1(10 Δ C,-G478C)-rOct1(10 Δ C), and rOct1(10 Δ C,G478C)-rOct1(10 Δ C,G478C).

Constructs for Cell-free Expression and Oligomerization—rOct1 and rOct1 mutants rOct1(rOat1-l), rOct1(G159V, G163V), rOct1(2 Δ C-l), and rOct1(6 Δ C-l) with a His tag at their C termini were made by PCR covering the complete coding

region without initiation and stop codons. PCR was performed as described (7). PCR amplicates were cloned into BamHI and XhoI sites of the pET21a vector, conserving the open reading frame with T7 tag and His tag of the vector. The rOct1-FLAG, rOct1(rOat1-l)-FLAG, and rOct1(6 Δ C-l)-FLAG in vector pET21a were obtained by substituting the 3'-terminal parts of rOct1-His, rOct1(rOat1-l)-His, and rOct1(6 Δ C-l)-His in the pET21a vector with the corresponding parts of the rOct1-FLAG, rOct1(rOat1-l)-FLAG, and rOct1(6 Δ C-l)-FLAG constructs in pRSSP. Constructs were sequenced to rule out PCR errors.

Constructs for Stable Expression in Human Embryonic Kidney 293 (HEK293) Cells for Transport Measurements—The construct rOct1/pRcCMV has been described earlier (15). The eukaryotic expression plasmids rOct1(rOat1-l)/pRcCMV and rOct1(6 Δ C-l)/pRcCMV were made by replacing the HindIII/NheI fragments of rOct1/pRcCMV with the respective fragment of the mutant transporters.

Constructs for Transient Expression in HEK293 Cells for Fluorescence Resonance Energy Transfer (FRET) Measurements—Fusion proteins of rOct1, rOct1(rOat1-l), and rOct1(6 Δ C-l) bearing cyan fluorescent protein (CFP) or yellow fluorescent protein (YFP) at their N termini (rOct1-C, rOct1-Y, rOct1(rOat1-l)-C, rOct1(rOat1-l)-Y, rOct1(6 Δ C-l)-C, and rOct1(6 Δ C-l)-Y) were prepared using the overlap extension PCR (18) and cloned into the HindIII/XhoI sites of the vector pcDNA3.1. The resulting constructs comprise the complete ORF of the fluorescent proteins connected by a short (two amino acids) linker to the ORF of rOct1 variants without their initiation codon.

Cell-free Expression of Transport Proteins—Cell-free expression was performed in the continuous exchange mode using bacterial extracts from *Escherichia coli* strain A19 as described (12, 19). Reaction mixture and feeding mixture were composed as described (19). Protein synthesis was performed in the absence of detergent in 1-ml dialysis tubes containing a membrane with a cut-off of 25 kDa (dialyzers obtained from Spectrum Laboratories Inc., Breda, The Netherlands). The dialyzers were rotated for 20 h at 30 °C in tubes containing 17 ml of feeding mixture. Precipitated proteins were spun down by a 10-min centrifugation at 10,000 \times g (4 °C). For purification of His-tagged proteins on Ni $^{2+}$ -NTA-agarose, pellets were washed with Tris buffer (20 mM Tris-HCl, pH 8, 500 mM NaCl) containing 10 mM imidazole. For purification of FLAG-tagged proteins using anti-FLAG-antibody coupled to agarose, washing was performed with Hepes buffer (20 mM Hepes-NaOH, pH 7.5, 150 mM NaCl). The washed precipitates were solubilized by incubation for 1 h at 30 °C with 1 ml of 2% (w/v) 1-myristoyl-2-hydroxy-*sn*-glycero-3-(phospho-*rac*-(1-glycerol)) (LMPG) dissolved in Tris buffer containing 10 mM imidazole (His-tagged transporters) or in Hepes buffer (FLAG-tagged transporters). The suspensions were centrifuged for 10 min at 10,000 \times g (4 °C), and the supernatants (LMPG supernatants) were used for purification.

Affinity Purification of Transporters—Purification was performed as described previously (12). Briefly, for purification on Ni $^{2+}$ -NTA-agarose, 1 ml of LMPG supernatant was mixed with 11 ml of Tris buffer containing 10 mM imidazole plus 1% (w/v)

Oligomerization of Organic Cation Transporter 1

CHAPS and Ni^{2+} -NTA-agarose and incubated for 1 h at 4 °C. The suspension was poured into a column and washed with 10 ml of Tris buffer containing 1% CHAPS and 10 mM imidazole. After additional washing in the presence of 1% CHAPS and 20 mM imidazole, proteins were eluted with 5 ml of Tris buffer containing 1% CHAPS and 100 mM imidazole. For immunopurification, 1 ml of LMPG supernatant was mixed with 10.5 ml of Hepes buffer containing 1% CHAPS and agarose beads coupled to anti-FLAG-antibody. The suspension was incubated overnight at 4 °C. The beads were separated by 10 min of centrifugation at $500 \times g$ and washed with Hepes-CHAPS, and transport proteins were eluted by overnight incubation at 4 °C with 1 ml of Hepes-CHAPS containing 0.2 mg/ml antigenic FLAG peptide. Beads were removed by 10 min of centrifugation at $500 \times g$.

Coprecipitation of His-tagged and FLAG-tagged Transporters—Coprecipitation was performed as described (12). LMPG supernatants (100 μl of each containing 20 μg of *in vitro* expressed His-tagged or FLAG-tagged transporter, 2% LMPG, and 10 mM imidazole) were mixed and diluted with 200 μl of Tris buffer containing 1% CHAPS and 10 mM imidazole (final concentration of 1% LMPG and 0.5% CHAPS). After a 1-h incubation at 4 °C, 100 μl of Ni^{2+} -NTA-agarose equilibrated with Tris buffer containing 1% CHAPS and 10 mM imidazole were added. The suspension was incubated for 1 h at 4 °C, and the beads were separated by a 10-min centrifugation at $500 \times g$. The beads were washed five times at room temperature with 1 ml of Tris buffer containing 1% CHAPS and 10 mM imidazole and five times with Tris buffer containing 1% CHAPS and 20 mM imidazole. For protein elution, pelleted beads were suspended for 10 min at room temperature in 400 μl of Tris buffer containing 1% CHAPS and 100 mM imidazole, and the suspension was centrifuged for 10 min at $500 \times g$. The supernatants were collected, and FLAG-tagged transporters were analyzed by Western blots.

Gel Filtration of rOct1—Each analysis was performed in the absence or presence of 10 mM dithiothreitol (DTT) using a 40- μl sample containing 160 μg of rOct1 protein, which was solubilized with 2% (w/v) LMPG. The running buffers without or with 10 mM DTT contained 20 mM Tris-HCl, pH 8.0, 500 mM NaCl, and either 1% (w/v) CHAPS or 0.5% (w/v) LMPG plus 0.5% (w/v) CHAPS. Protein samples were applied to a Superdex 200 PC 3.2/30 column in a SMART system (GE Healthcare) or to a tandem of two coupled Superose 6 PC 3.2/30 columns in an ÄKTAmicro™ system (GE Healthcare). After equilibration of the columns, gel filtration was performed with a flow rate of 50 $\mu\text{l}/\text{min}$ (Superdex 200 column) or of 280 $\mu\text{l}/\text{min}$ (Superose 6 columns). The systems were calibrated with ferritin (440 kDa), aldolase (158 kDa), conalbumin (75 kDa), ovalbumin (43 kDa), and ribonuclease A (14 kDa) supplied by GE Healthcare.

SDS-PAGE and Western Blotting—For SDS-PAGE, protein samples were pretreated for 30 min at 37 °C in 60 mM Tris-HCl, pH 6.8, containing 2% (w/v) SDS, and 7% (v/v) glycerol. The pretreatment was performed in the presence or absence of 100 mM DTT. SDS-PAGE was performed as described (20). Separated proteins were transferred by electroblotting to a polyvinylidene difluoride membrane. For immunostaining, anti-FLAG antibody raised in mice diluted 1:20,000 (Sigma-Aldrich)

and successively anti-mouse IgG coupled to horseradish peroxidase (HRP) diluted 1:5,000 (Sigma-Aldrich) were used. Binding of HRP-coupled antibodies was visualized using enhanced chemiluminescence (ECL system, GE Healthcare). Prestained molecular weight markers (BenchMark, Invitrogen) were used to determine apparent molecular masses.

Preparation of Protein-Lipid Aggregates—1 mg of cholesterol, 1 mg of phosphatidylcholine, and 1 mg of phosphatidylserine were dissolved in 1 ml of a chloroform/methanol mixture (1:1, v/v) and dried in a round bottom flask under a stream of nitrogen, and 500 μl of purified transporter proteins solubilized in Tris buffer containing 1% CHAPS and 100 mM imidazole were added. The round bottom flasks were shaken for 1 h at 4 °C, and CHAPS was removed by dialysis at 4 °C against 20 mM Tris/HCl, pH 7.9, 500 mM NaCl, and 100 mM choline chloride. The obtained suspensions were centrifuged for 30 min at $200,000 \times g$ (4 °C). The sediments were resuspended in 2 ml of ice-cold KC buffer (20 mM imidazole, pH 7.4, 0.1 mM Mg^{2+} , 100 mM K^+ , 100 mM cyclamate⁻). After another 30-min centrifugation at $200,000 \times g$, the sediments were suspended in 150 μl of KC buffer. The protein-lipid aggregates were used for binding measurements and for preparation of large proteoliposomes.

Preparation of Large Proteoliposomes—Reconstitution of purified transporters into large proteoliposomes was performed using a freeze-thaw procedure (12). Large multilamellar liposomes were mixed with protein-lipid aggregates, and the mixture was frozen and thawed, pelleted, and homogenized. To prepare large multilamellar liposomes, 4 mg of phosphatidylserine and 2 mg of cholesterol in 1 ml of chloroform/methanol (1:1, v/v) were dried in a round bottom flask under a stream of nitrogen. 1 ml of KC buffer was added, and the flask was shaken for 3 h at room temperature under nitrogen. Large lipid aggregates were pelleted by 10-min centrifugation at $10,000 \times g$ at room temperature, and multilamellar liposomes in the supernatant were concentrated by centrifugation at $200,000 \times g$ for 15 min and resuspension of the pellet in 150 μl of KC buffer (room temperature). To form large proteoliposomes, 150 μl of the protein-lipid aggregates were mixed with 150 μl of the multilamellar liposomes and incubated for 15 min at 41 °C. This mixture was snap-frozen in liquid nitrogen. Shortly before transport measurements were started, the sample was thawed by a 5-min incubation at 37 °C in a water bath. After the addition of 1.7 ml of KC buffer (room temperature), the proteoliposomes were spun down by centrifugation at $200,000 \times g$ for 15 min (room temperature). The pellet was suspended in 300 μl of KC buffer (room temperature), and formation of monolamellar proteoliposomes was induced by repeated suction of the suspension into and forced extrusion out of a 100- μl pipette tip.

Measurement of MPP⁺ Binding to Protein-Lipid Aggregates—Binding measurements were performed at 0 °C to avoid contribution of MPP⁺ uptake and to reduce dissociation of MPP⁺ during washing. Assuming that the rate constants for association and dissociation of MPP⁺ have a similar temperature dependence, similar dissociation constant (K_D) values are expected at 0 and 37 °C. 10 μl of ice-cold protein-lipid aggregates were mixed with 90 μl of ice-cold KC buffer containing 12 nM [³H]MPP⁺ without or with different concentrations of non-

radioactive MPP⁺. After incubation for 10 min at 0 °C, the protein-lipid aggregates were applied to 0.22- μ m cellulose acetate filters (Millipore GSWP) and washed with 10 ml of ice-cold KC buffer. The filters were dissolved in LUMASAFETM PLUS mixture (Lumac LSC, Groningen, The Netherlands) and assayed for radioactivity.

Measurement of MPP⁺ Uptake into Large Proteoliposomes—For measurements of MPP⁺ uptake, large proteoliposomes filled with KC buffer were preincubated for 10 min at 37 °C in the absence or presence of 20 μ M valinomycin. The preincubation was performed without or with a 100 μ M concentration of the OCT inhibitor quinine (1). Uptake was initiated by mixing 10 μ l of prewarmed proteoliposomes (37 °C) with 90 μ l of prewarmed (37 °C) NaC buffer (20 mM imidazole, pH 7.4, 0.1 mM Mg²⁺, 100 mM Na⁺, 100 mM cyclamate⁻) containing 12 nM [³H]MPP⁺ without or with non-radioactive MPP⁺, TEA⁺, tetrabutylammomium (TBuA⁺), or tetrapentylammomium (TPeA⁺). After incubation for 1 s, uptake was stopped by adding 1 ml of ice-cold stop solution (KC buffer containing 100 μ M quinine). An accurate 1-s incubation was achieved by placing the proteoliposomes on the inner wall of the reaction tube just above the incubation buffer. Uptake was started by moving the tube close to a switched-on vortexer and immediately stopped with stop solution from a prepositioned pipette. The 1-s incubation time was determined using a metronome. For measurement of radioactivity within proteoliposomes, the proteoliposomes suspended in stop solution were applied to 0.22- μ m cellulose acetate filters (Millipore GSWP) and washed with 10 ml of ice-cold stop solution. The filters were dissolved and assayed for radioactivity as described above.

FRET Microscopy—FRET (21) was measured with a Carl Zeiss Axiovert 200 epifluorescence microscope using the “three-filter method” (22). Images were taken using $\times 63$ oil immersion objectives and filter wheels from Ludl Electronic Products allowing a rapid excitation and emission filter exchange. We investigated HEK293 cells, which were transiently transfected with plasmid cDNA (1.7 μ g/ μ l) using the calcium phosphate coprecipitation method (23). The filter wheels were configured as follows: CFP (I_{donor} ; excitation, 436 nm; emission, 480 nm; dichroic mirror, 455 nm); YFP (I_{acceptor} ; excitation, 500 nm; emission, 535 nm; dichroic mirror, 515 nm); and FRET (I_{FRET} ; excitation, 436 nm; emission, 535 nm; dichroic mirror, 455 nm). Images were taken with a CCD camera (Coolsnap fx, Roper Scientific). Background fluorescence was subtracted from all images. Images were analyzed pixel by pixel using ImageJ, version 1.43b (Wayne Rassband, National Institutes of Health) and the ImageJ plug-in PixFRET (Pixel by Pixel analysis of FRET with ImageJ, version 1.5.0) (24). Spectral bleed-through parameters for the donor bleed-through (BT_{donor}) and the acceptor bleed-through (BT_{acceptor}) were determined, and N_{FRET} was calculated in the following way.

$$N_{\text{FRET}} = \frac{I_{\text{FRET}} - BT_{\text{donor}} \times I_{\text{donor}} - BT_{\text{acceptor}} \times I_{\text{acceptor}}}{\sqrt{I_{\text{donor}} \times I_{\text{acceptor}}}} \times 100 \quad (\text{Eq. 1})$$

The mean N_{FRET} was measured at the plasma membrane (predefined as the region of interest) using the computed N_{FRET}

image. The regions of interest were selected in the CFP (donor) or YFP (acceptor) image (to avoid bleaching-associated bias) and transmitted to the N_{FRET} image by the ImageJ Multi Measure Tool. As a negative control, we employed the CFP-labeled form of rOct1 (C-Oct1) with a membrane-bound form of YFP (25) that was kindly provided by Viacheslav Nikolaev (University of Würzburg).

Transport Studies in HEK293 Cells Stably Transfected with rOct1—Uptake of [³H]MPP⁺ was measured into HEK293 cells stably transfected with rOct1 (26). Confluent cells were washed with Dulbecco's phosphate-buffered saline (D-PBS), suspended by shaking, and collected by 10-min centrifugation at 1,000 \times g. Cells were either directly used for transport measurements (control) or incubated for 6 min at 37 °C with D-PBS containing 10 mM DTT or with D-PBS containing 0.1 mM DTT (0.1 mM DTT control). DTT-treated cells were sedimented by centrifugation, washed two times at room temperature with D-PBS containing 0.1 mM DTT, and suspended at 37 °C in D-PBS containing 0.1 mM DTT. For uptake measurement, cells were incubated for 1 s with D-PBS containing 0.1 μ M [³H]MPP⁺ plus various concentrations of non-radioactive MPP⁺. Uptake was stopped by the addition of ice-cold D-PBS containing 100 μ M quinine⁺ (stop solution). Cells were washed three times with ice-cold stop solution, solubilized with 4 M guanidine thiocyanate, and analyzed for radioactivity.

In Vitro Synthesis of cRNA—For injection into *X. laevis* oocytes, m7G(5')G-capped cRNA was prepared, purified, and stored as described previously (27, 28). To prepare sense cRNA from rOct1 (4), rOct1 mutants, or rOct1 tandem protein, the respective purified plasmids were linearized with MluI. cRNA was synthesized using SP6 RNA polymerase employing the “mMESSAGE mMACHINE” kit (Ambion, Huntingdon, UK). cRNA concentrations were estimated from ethidium bromide-stained agarose gels using polynucleotide marker as a standard (29).

Expression of rOct1 and Mutants in Oocytes of X. laevis—*X. laevis* oocytes were prepared and stored in Ori buffer (5 mM MOPS, 100 mM NaCl, 3 mM KCl, 2 mM CaCl₂, and 1 mM MgCl₂, adjusted to pH 7.4 using NaOH) supplemented with 50 mg/liter gentamycin as described (30). Per oocyte, 50 nl of H₂O containing 10 ng of cRNA encoding for wild-type rOct1, rOct1 mutants, or rOct1 chimeras were injected. For expression, oocytes were then stored for 2 or 3 days in Ori buffer at 16 °C.

Inhibition of Transport Activity by Covalent Modification of Cysteine 478—To inactivate rOct1(10 Δ C,G478C) expressed individually or within tandem proteins, oocytes were incubated for 10 min with 100 μ M MTSET. Thereafter, the oocytes were washed at least three times with Ori buffer at room temperature.

Tracer Uptake Measurements in Oocytes—Oocytes expressing rOct1, rOct1 mutants, and rOct1 tandem proteins were incubated for 15 min at room temperature in Ori buffer containing [¹⁴C]TEA⁺ or [³H]MPP⁺. Substrate dependence of uptake was determined by measurements in the presence of different concentrations of nonradioactive TEA⁺ or MPP⁺. Correction for nonspecific uptake plus nonspecific adsorption to the cell surface was performed by subtracting radioactivity associated with non-injected oocytes from the same batch.

Oligomerization of Organic Cation Transporter 1

Nonspecific uptake plus nonspecific adsorption of [^{14}C]TEA $^+$ and [^3H]MPP $^+$ was always less than 10% of the specific uptake. After incubation for uptake, the oocytes were washed three times with ice-cold Ori buffer and solubilized by using 5% SDS solution, and the intracellular radioactivity was analyzed by liquid scintillation counting.

Quantification and Statistics—The software package GraphPad Prism version 4.1 (GraphPad Software, San Diego, CA) was used to compute statistical parameters. Quantification of staining in Western blots, MPP $^+$ binding measurements to precipitated proteins, and uptake measurements in proteoliposomes are presented as mean values \pm S.D. Uptake measurements in oocytes and N_{FRET} values are presented as mean values \pm S.E. Staining of proteins in Western blots was quantified by densitometry as described (12). Apparent K_m values of individual experiments were determined by fitting the Michaelis-Menten equation to the data. For inhibition of tracer cation uptake by nonlabeled cations IC_{50} values of individual experiments were calculated by fitting the Hill equation to the data. Because the MPP $^+$ concentrations employed for inhibition studies were at least 10 times smaller compared with the K_m value for MPP $^+$, the IC_{50} values are practically identical to K_i values. In Fig. 1 and Tables 1 and 2, an analysis of variance test with *post hoc* Tukey comparison was used to test the significance of differences between groups. The statistical significance of differences between the experimental conditions in Figs. 7 and 8 was examined using the Kruskal-Wallis test followed by Dunn's multiple comparison test. The significance of effects of single point mutations on inhibition of transport activity by MTSET in Fig. 10 was analyzed by Student's *t* test.

RESULTS

The Large Extracellular Loop of rOct1 Is Required for Plasma Membrane Targeting—Previously, we observed that replacement of individual cysteine residues in the large extracellular loop connecting TMH1 and -2 by serine residues resulted in failure of these constructs to induce TEA $^+$ uptake in oocytes of *X. laevis* (17). When the large extracellular loop of rOct1 was replaced by the respective loop of rOct2 (rOct1(rOct2-l)), uptake of 9 μM TEA $^+$ was slightly smaller compared with rOct1 wild type, and no significant TEA $^+$ uptake was detected when it was replaced by the respective loop of rat organic anion transporter rOat1 (rOct1(rOat1-l)) (Fig. 1A, left). At variance to TEA $^+$ uptake, some uptake of MPP $^+$ was expressed by rOct1(rOat1-l) (Fig. 1A, right). In Fig. 1B, we measured the substrate dependence of MPP $^+$ uptake by rOct1, rOct1(rOct2-l), rOct1(rOat1-l), and a rOct1 mutant where the six cysteine residues in the large extracellular loop were replaced by serine residues (rOct1(6 Δ C-l)). In chimera rOct1(rOct2-l) the maximal velocity of transport for MPP $^+$ (V_{max}) measured at saturated substrate concentration and calculated by the Michaelis-Menten equation was reduced about 50% compared with rOct1 wild type, whereas it was reduced 85% in chimera rOct1(rOat1-l) and 90% in Oct1(6 Δ C-l). The Michaelis-Menten constant (K_m) value of rOct1(rOct2-l) was similar to rOct1 wild type; however, the K_m values of chimeras rOct1(rOat1-l) and Oct1(6 Δ C-l) were increased about 3-fold. To determine whether the reduced cation transport expressed by chimeras

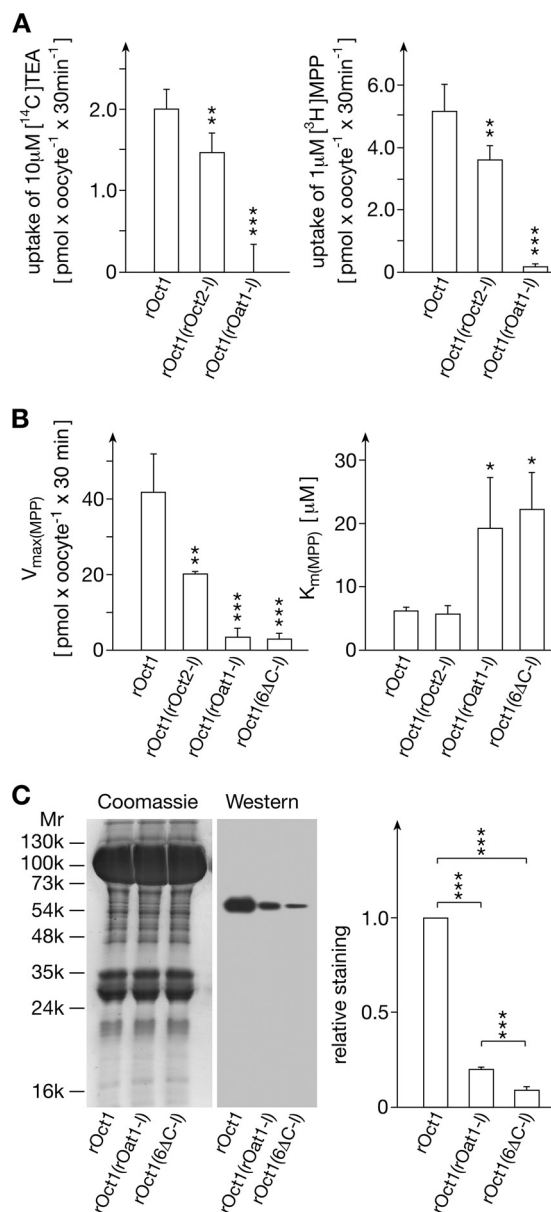


FIGURE 1. Mutations within the large extracellular loop of rOct1 alter functional properties and plasma membrane targeting. A, changes of the uptake of 10 μM TEA $^+$ and 1 μM MPP $^+$ after replacement of the large extracellular loop of rOct1 by the respective loops of rOct2 (rOct1(rOct2-l)) or rOat1 (rOct1(rOat1-l)). rOct1 wild type and the chimeras were expressed in oocytes of *X. laevis*, and the expressed uptake rates were measured. Mean values \pm S.D. (error bars) of three experiments using 24–30 experiments are indicated. B, changes of the substrate dependence of MPP $^+$ uptake after mutations in the large extracellular loop of rOct1. rOct1 wild type, the chimera rOct1(rOct2-l) and rOct1(rOat1-l), and a mutant in which the six cysteines in the large extracellular loop of rOct1 were replaced by serines (rOct1(6 Δ C-l)), were expressed in oocytes, and the substrate dependences of MPP $^+$ uptake were measured. The Michaelis-Menten equation was fitted to the data, and V_{max} and apparent K_m values were calculated. Mean values \pm S.D. of three experiments are indicated. C, changes of transporter proteins within the plasma membranes after mutations in the large extracellular loop of rOct1. FLAG-tagged rOct1 wild type and rOct1 mutants were expressed in oocytes, and the plasma membranes were purified by adsorption to colloidal silica. Plasma membrane proteins were separated by SDS-PAGE and blotted to polyvinylidene difluoride membranes, and Western blots were stained with an anti-FLAG antibody. Antibody staining after enhanced chemiluminescence reaction was quantified by densitometry. 30 μg of protein were applied per lane. Mean values \pm S.D. of three experiments are indicated. *, $p < 0.05$; **, $p < 0.01$; ***, $p < 0.001$, analysis of variance test with *post hoc* Tukey comparison.

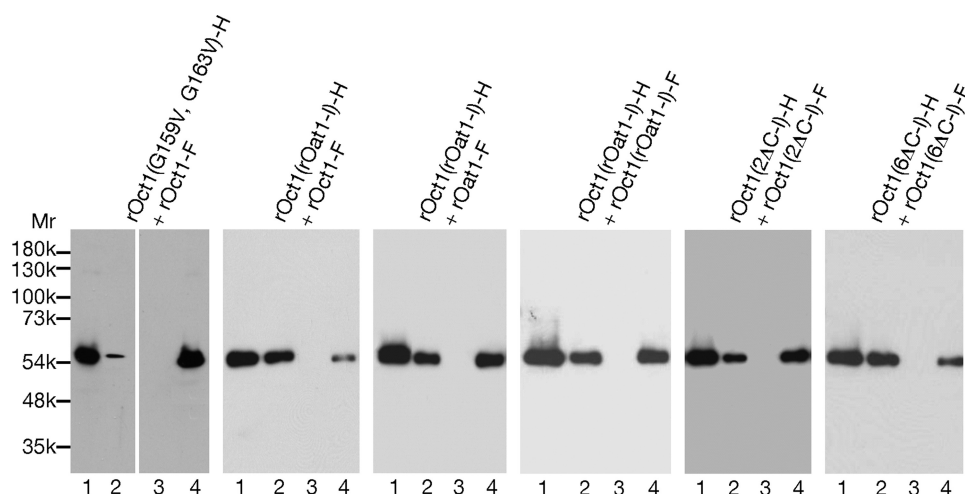


FIGURE 2. Interaction of solubilized transporters in the presence of LMPG and CHAPS. LMPG supernatants (100 μ l each, containing 2% LMPG, 10 mM imidazole, and a His-tagged rOct1 transporter mutant (rOct1(G159V,G163V)-H, rOct1(rOat1-l)-H, rOct1(2 Δ C)-H, or rOct1(6 Δ C)-H) or a FLAG-tagged transporter (rOct1-F, rOat1-F, rOct1(Oat1-l)-F, rOct1(2 Δ C)-F, or rOct1(6 Δ C)-F) were mixed. The samples were diluted with 200 μ l of Tris buffer containing 1% CHAPS and 10 mM imidazole (lanes 1). After a 1-h incubation at 4 $^{\circ}$ C, Ni²⁺-NTA-agarose beads were added, the suspension was incubated for 1 h and centrifuged, and the supernatant (lanes 2) was removed. The beads were washed five times with 1 ml of buffer containing 1% CHAPS and 10 mM imidazole and pelleted (supernatant lanes 3). His-tagged proteins were eluted by incubating the beads with 400 μ l of buffer containing 1% CHAPS and 100 mM imidazole (supernatant lanes 4). Proteins were separated by SDS-PAGE, transferred to a blotting membrane, and stained with an antibody against the FLAG tag. Per lane, 5 μ l of sample were applied.

rOct1(rOat1-l) and rOct1(6 Δ C-l) was due to reduction of transporter protein in the plasma membrane, we expressed FLAG-tagged rOct1 wild type and FLAG-tagged mutants rOct1(rOat1-l) and rOct1(6 Δ C-l) in oocytes, purified the plasma membranes by adsorption to colloidal silica (31), separated the plasma membrane proteins by SDS-PAGE, and identified the transporters in Western blots using anti-FLAG antibody (Fig. 1C). Quantification of antibody staining revealed a reduction of $80 \pm 1\%$ (rOct1(rOat1-l)) and $91 \pm 0.1\%$ (rOct1(6 Δ C-l)) compared with rOct1 wild type. The data indicate that replacement of the large extracellular loop of rOct1 by the respective loop of rOat1 or exchange of the six cysteine residues within the loop lead to largely decreased amounts of transporters in the plasma membrane, suggesting targeting defects. Misfolding and/or failure of oligomerization in the endoplasmic reticulum may be the reason for disturbed targeting to the plasma membrane (32, 33). Because it has been shown that OATs and OCTs form homo-oligomers (11–13), we tested whether the large extracellular loop of rOct1 is important for oligomerization.

The Large Extracellular Loop of rOct1 Is Required for Homo-oligomerization—We previously observed homo-oligomerization of solubilized rOct1 and rOat1 but did not detect significant oligomerization between rOct1 and rOat1 (12). To determine whether the large extracellular loop of rOct1 is important for oligomerization, we synthesized and solubilized His-tagged and FLAG-tagged rOct1 and rOat1 mutants separately and analyzed them for oligomerization as described previously (12). We mixed the transporters solubilized with 2% LMPG with the same volume of buffer containing 1% CHAPS, added Ni²⁺-NTA-agarose beads, pelleted the beads, washed them, and detached the proteins from the beads. Previously, we described that $93 \pm 2\%$ of FLAG-tagged rOct1 wild type was coprecipitated with His-tagged rOct1 wild type and that 100% of FLAG-tagged rOat1 wild type was coprecipitated with His-

TABLE 1

Coprecipitation of solubilized FLAG-tagged and His-tagged transporters

The indicated FLAG-tagged and His-tagged transporters were expressed separately, solubilized with 2% LMPG, mixed, and diluted with an equal volume of buffer containing 1% CHAPS. Precipitation was performed with Ni²⁺-NTA-agarose, and coprecipitated FLAG-tagged transporters were quantified in Western blots. In rOct1, DTT, the precipitation was performed in the presence of 10 mM DTT. Mean values of three experiments \pm S.D. are shown.

Construct		Coprecipitation of FLAG-tagged construct (percentage of total)
His-tagged	FLAG-tagged	
%		
rOct1 ^a	rOct1	93.3 \pm 2.1 ^c
rOct1 ^a	rOat1	12.3 \pm 2.5 ^b
rOct1 (rOat1-l)	rOct1	10.7 \pm 2.5 ^b
rOct1 (rOat1-l)	rOat1	58.3 \pm 6.1 ^{b,c}
rOct1 (rOat1-l)	rOct1 (rOat1-l)	61.0 \pm 4.6 ^{b,c}
rOct1 (6 Δ C-l)	rOct1 (6 Δ C-l)	21.7 \pm 5.1 ^b
rOct1 (2 Δ C-l)	rOct1 (2 Δ C-l)	86.3 \pm 3.5 ^c
rOct1 (1–177)	rOct1 (1–177)	2.0 \pm 1.0 ^b
rOct1, DTT	rOct1, DTT	4.3 \pm 1.5 ^b

^a Data are taken from Ref. 12.

^b $p < 0.001$ for difference to homo-oligomerization of OCT1.

^c $p < 0.001$ for difference to hetero-oligomerization of rOct1 with rOat1.

tagged rOat1 wild type, whereas only $12.3 \pm 2.5\%$ of rOat1 was coprecipitated with rOct1 (see Fig. 4 in Ref. 12). Homo-oligomerization was not disturbed when two glycine residues within a predicted oligomerization motif in TMH2 of rOct1 (GXXXG) (34) were exchanged by valine residues (rOct1(G159V,G163V)) (Fig. 2). Interestingly, with His-tagged rOct1 mutant containing the large extracellular loop of rOat1 (rOct1(rOat1-l)), only $10.7 \pm 2.5\%$ of FLAG-tagged rOct1 wild type was coprecipitated (Fig. 2 and Table 1). At variance with His-tagged rOct1(Oat1-l), $58.3 \pm 6.1\%$ of FLAG-tagged rOat1 and $61.0 \pm 4.6\%$ FLAG-tagged rOct1(rOat1-l) were coprecipitated (Fig. 2 and Table 1). The data indicate that the large extracellular loops of rOct1 or rOat1 are pivotal for oligomerization. The large extracellular loops of rOct1 and rOat1 contain four cysteine residues in corresponding positions, and rOct1 con-

Oligomerization of Organic Cation Transporter 1

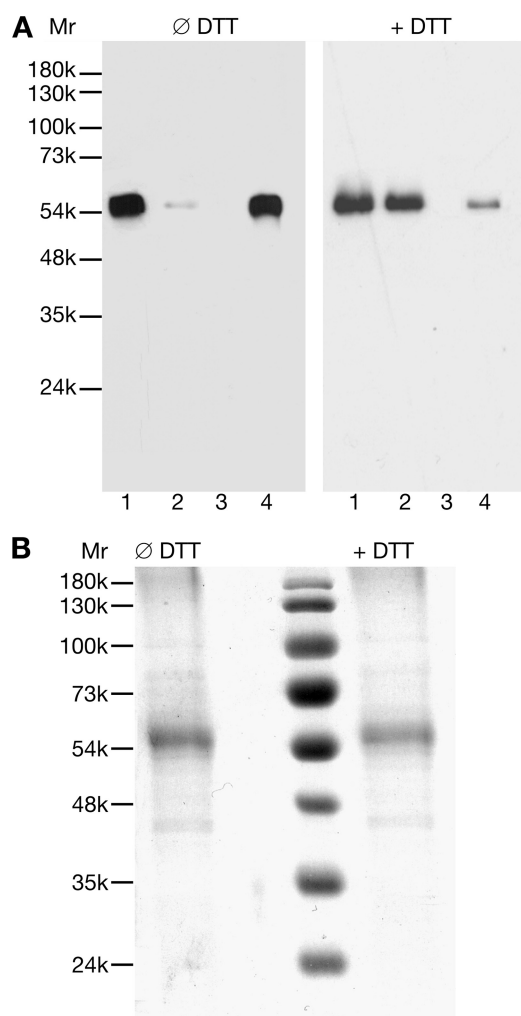


FIGURE 3. Homo-oligomerization of solubilized rOct1 in the presence of LMPG and CHAPS is prevented by reduction of intramolecular disulfide bridge(s). *A*, effect of DTT on coprecipitation of solubilized FLAG-tagged rOct1 wild type with solubilized His-tagged rOct1. The experimental protocol described in the legend to Fig. 2 was used, and the data are presented as in Fig. 2. Coprecipitation of solubilized proteins in the presence of LMPG plus CHAPS was performed without DTT and with 10 mM DTT in the solubilization buffer. *B*, exclusion of intermolecular disulfide bridges between rOct1 monomers. The mixtures of solubilized FLAG-tagged and His-tagged rOct1 wild type proteins used for coprecipitation in Fig. 3*A* were separated by SDS-PAGE either in the presence or absence of DTT in the sample buffer and stained with Coomassie Brilliant Blue.

tains two additional cysteine residues in positions 62 and 103. Homo-oligomerization was not disturbed when these latter cysteine residues were replaced by serines (rOct1-2ΔC) (Fig. 2 and Table 1). However, replacement of all six cysteine residues in the large extracellular loop of rOct1 (rOct1-6ΔC-1) largely reduced the oligomerization. Only 21.7 ± 5.1% of FLAG-tagged rOct1-6ΔC-loop was coprecipitated with His-tagged rOct1(6ΔC-1).

To test whether disulfide bridges are required for oligomerization, we measured oligomerization of rOct1 wild type in the absence and presence of the reducing agent DTT. DTT abolished oligomerization (Fig. 3*A* and Table 1). To determine whether the disulfide bonds required for oligomerization represent intra- or intermolecular bridges we performed SDS-PAGE of purified rOct1 in the absence and presence of DTT

(Fig. 3*B*). Under non-reducing and reducing conditions, one major band with an apparent molecular mass of 56 kDa representing the monomeric form of rOct1 was obtained. This excludes intermolecular disulfide bonds. The data suggest that the tertiary structure of the large extracellular loop is stabilized by intramolecular disulfide bonds and is required for oligomerization. We also investigated whether an N-terminal rOct1 fragment containing TMH1, the large extracellular loop, and TMH2 (rOct1 fragment 1–177) is capable of forming oligomers. This was not the case (Table 1), indicating that the loop structure is dependent on the positions of TMH1 and -2 within the transporter or that an additional domain(s) of rOct1 conserved in rOct1 and rOat1 is required for oligomerization.

Oligomerization of rOct1 in Solution Is Favored by LMPG—The above described precipitation assays, which were performed in the presence of 1% LMPG and 0.5% CHAPS, indicated that all rOat1 protein and more than 90% of rOct1 protein were present as homo-oligomers. At variance, gel filtration chromatography of rOat1, which was performed in the presence of 1% CHAPS, showed that less than 50% of rOat1 protein formed oligomers under these conditions (see Fig. 2*A* in Ref. 12). To determine the effect of detergents on oligomerization of rOat1, we also performed chromatography of rOat1 in presence of 0.5% CHAPS plus 0.5% LMPG using a Superdex 200 column. Under these conditions, the protein appeared in the void volume, indicating oligomerization (supplemental Fig. 1). If the same experiment was performed with 10 mM DTT in the running buffer, all protein entered the gel and eluted at a similar position as conalbumin (75 kDa), suggesting rOat1 monomers (61 kDa) with some bound detergent (supplemental Fig. 1). To investigate whether rOct1 shows a similar behavior, we analyzed rOct1 protein in the presence of 1% CHAPS (Fig. 4*A*) and in the presence of 0.5% LMPG plus 0.5% CHAPS (Fig. 4*B*) by size exclusion gel chromatography using a Superdex 200 column (Fig. 4*A*) or a Superose 6 column (Fig. 4*B*). In the presence of DTT, one main peak with an apparent molecular mass of ~75 kDa was observed under both conditions, indicating rOct1 monomers. In the absence of DTT and presence of 1% CHAPS, two peaks with molecular masses of ~75 and ~150 kDa were observed, suggesting monomers and dimers. In the absence of DTT and presence of 0.5% LMPG plus 0.5% CHAPS, no monomeric protein was observed, and rOct1 was eluted as a broad peak with the highest absorbance at 305 kDa, suggesting higher oligomers that may be unstable. The data suggest that oligomerization of solubilized rOct1 and rOat1 is detergent-dependent and favored by LMPG. They confirm the critical role of disulfide bridges for oligomerization.

Function of rOct1 Is Altered by Mutations within the Large Extracellular Loop Independently of Oligomerization Impairment—To determine whether functional activities of rOct1 are influenced by oligomerization, we measured MPP⁺ binding to precipitated proteins, MPP⁺ transport of reconstituted proteins, and inhibition of MPP⁺ transport by TEA⁺, TBuA⁺, and TPcA⁺. rOct1 wild type, the oligomerizing rOct1(Oat1-1) mutant and the non-oligomerizing rOct1-

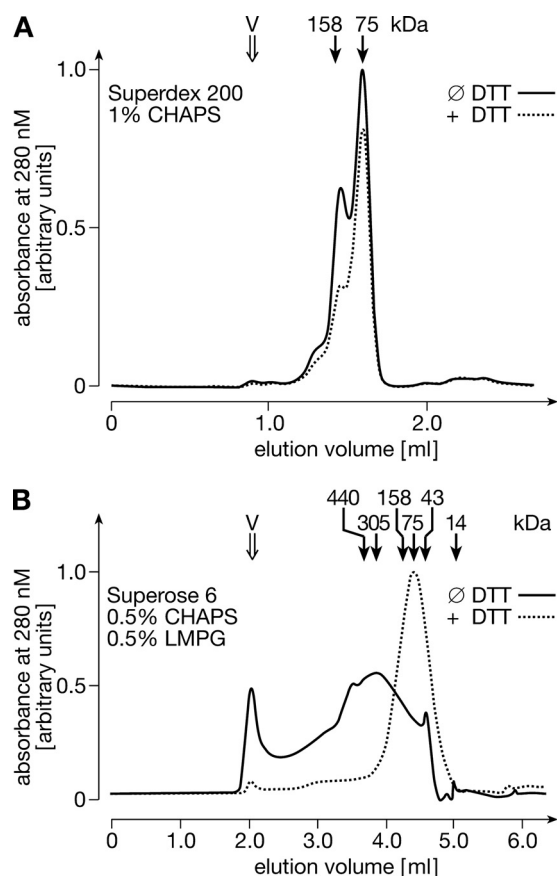


FIGURE 4. Gel filtration chromatography of solubilized rOat1 wild type in the presence of LMPG and CHAPS performed under non-reducing and reducing conditions. Cell-free expressed rOat1 protein was solubilized with 2% LMPG and concentrated to 4 mg/ml protein, and 40 μ l were applied to a Superdex 200 column (A) or to a tandem of two coupled Superose 6 PC 3.2/30 columns (B). The columns were equilibrated and operated with 20 mM Tris/HCl, pH 8, containing 500 mM NaCl and either 1% CHAPS (A) or 0.5% LMPG plus 0.5% CHAPS using a flow rate of 50 μ l/min (A) or 0.28 ml/min (B). In one series of experiments, 10 mM DTT was added to the sample buffer, and in another series of experiments, DTT was omitted. The indicated molecular weights were obtained by calibration of the columns with ferritin (440 kDa), aldolase (158 kDa), conalbumin (75 kDa), ovalbumin (43 kDa), and ribonuclease A (14 kDa). The data suggest that under non-reducing conditions, rOat1 wild type forms dimers in the presence of 1% CHAPS and tetramers in the presence of 0.5% CHAPS and 0.5% LMPG.

(6 Δ C-1) mutant were compared. MPP⁺ binding to precipitated transporters was measured at 0 °C (Fig. 5). The transporters were synthesized by cell-free expression, solubilized with 2% LMPG, purified in the presence of 1% CHAPS, and precipitated by detergent removal. In the precipitate, no quinine-inhibitable transport of [³H]MPP⁺ was detected at 37 °C; however, saturable binding of [³H]MPP⁺ could be measured at 0 °C. Similar total numbers of MPP⁺ binding sites (in nmol \times mg of protein⁻¹) were determined for rOat1 wild type (31.4 \pm 1.9), Oat1(Oat1-I) (28.3 \pm 4.8), and rOat1(6 Δ C-1) (31.7 \pm 2.7). Assuming that all precipitated transporter molecules are active, the data suggest that about 2 molecules of MPP⁺ bind per transporter monomer. The K_D values of rOat1(6 Δ C-1) (119 \pm 23 μ M) and rOat1(Oat1-I) (113 \pm 32 μ M) were similar but higher compared with rOat1 wild type (77 \pm 8.6 μ M). Because binding of MPP⁺ to rOat1 wild type and the rOat1 mutants could be fitted with a one-binding site model, the affinities of

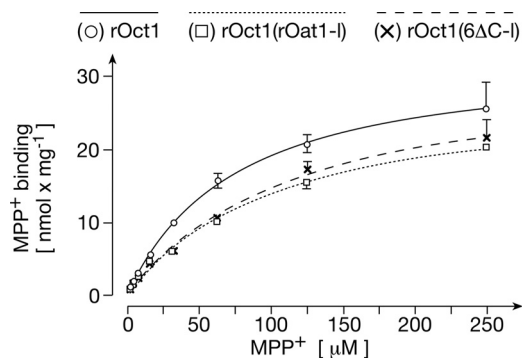


FIGURE 5. Comparison of MPP⁺ binding to rOat1, rOat1(rOat1-I), and rOat1(6 Δ C-1). Binding of [³H]MPP⁺ was measured to rOat1 (○, solid line), rOat1(rOat1-I) (□, dotted line), and rOat1(6 Δ C-1) (×, dashed line). The transporters were synthesized by cell-free expression, solubilized with LMPG, purified in the presence of CHAPS, and precipitated by detergent removal via dialysis. Binding of 12 nM [³H]MPP⁺ was measured in the presence of the indicated total MPP⁺ concentrations and in the presence of 5 mM nonradioactive MPP⁺. [³H]MPP⁺ binding replaced by 5 mM MPP⁺ was calculated. Mean values \pm S.D. from four parallel measurements of three typical experiments are indicated. A one-site binding curve was fitted to the data. The K_D values of 119 \pm 23 μ M (rOat1(6 Δ C-1)), 113 \pm 32 μ M (rOat1(Oat1-I)), and 77 \pm 8.6 μ M (rOat1 wild type) were obtained. The difference between rOat1 wild type and rOat1(6 Δ C-1) was significant in Student's *t* test (p < 0.05).

the two assumed MPP⁺ binding sites per monomer may be similar.

When the precipitated transporters were reconstituted into large proteoliposomes using a freeze-thaw procedure (12), transporter-mediated, quinine-inhibited MPP⁺ uptake could be measured at 37 °C (Fig. 6). Measuring the concentration dependence of MPP⁺ uptake, about 2 times lower V_{max} values were determined for rOat1(Oat1-I) and rOat1(6 Δ C-1) versus rOat1 wild type. At variance, about 3 times higher apparent K_m values were determined for rOat1(Oat1-I) and rOat1(6 Δ C-1) versus rOat1 wild type (Fig. 6A and Table 2). Importantly, neither the V_{max} values nor the K_m values differed between the oligomerizing rOat1(Oat1-I) mutant and the non-oligomerizing rOat1(6 Δ C-1) mutant. Similar affinities were obtained for inhibition of MPP⁺ uptake by TEA⁺, TBuA⁺, and TPeA⁺ (Fig. 6, B–D, and Table 2). The affinities of TEA⁺ and TBuA⁺ to inhibit uptake of 0.1 μ M MPP⁺ by rOat1(Oat1-I) and rOat1(6 Δ C-1) were very similar but about 15% lower compared with rOat1 wild type. For inhibition of MPP⁺ uptake by TPeA⁺, similar affinities were observed for rOat1(Oat1-I), rOat1(6 Δ C-1), and rOat1 wild type. The data indicate that mutations in the large extracellular loop may change substrate binding, turnover, and substrate dependence of organic cation transport. These effects on transport activities appear to be due to structural changes within the loop but are probably not correlated with oligomerization.

Oligomerization of rOat1 Wild Type, rOat1(rOat1-I), rOat1(6 Δ C-1), and DTT-treated rOat1 Wild Type in Vivo—To evaluate whether the effects on oligomerization observed with solubilized rOat1 wild type and mutants in the presence of LMPG are representative of the situation in the plasma membrane, we employed FRET microscopy (21) using the three-filter method according to Xia and Liu (35) (Figs. 7 and 8). rOat1 or rOat1 mutants that were N-terminally labeled with CFP and YFP were coexpressed in HEK293 cells. Quantitative

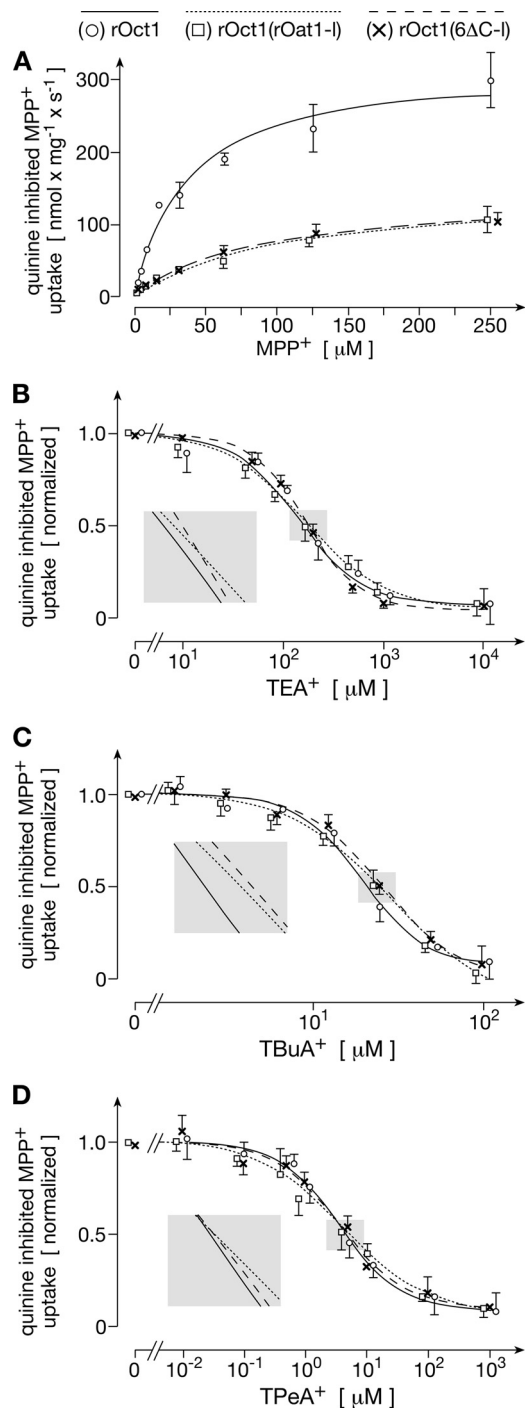


FIGURE 6. Comparison of MPP⁺ uptake into proteoliposomes containing rOct1, rOct1(rOat1-l), and rOct1(6ΔC-l). His-tagged transporters were expressed *in vitro* and purified, and 60 μg of individual transporters were reconstituted into proteoliposomes containing 100 mM potassium cyclamate. After preincubation with valinomycin, proteoliposomes were incubated for 1 s with 12 nM [³H]MPP⁺ plus various concentrations of nonlabeled MPP⁺ (A) TEA⁺ (B), TBuA⁺ (C), or TPpA⁺ (D). The incubation buffer contained 90 mM Na⁺, 10 mM K⁺, and 100 mM cyclamate⁻. Measurements were performed in the absence and presence of 100 μM quinine, and quinine-inhibited uptake is indicated. Means ± S.D. (error bars) of three measurements from individual experiments are shown. The Michaelis-Menten equation was fitted to the data in A, whereas the Hill equation was fitted to the data in B–D. In the insets, fitted curves close to the calculated IC₅₀ values are enlarged.

visualization of protein oligomerization was achieved by the method of Feige *et al.* (24), which generates N_{FRET} images (Fig. 7A). After coexpression of CFP-rOct1 wild type/YFP-rOct1 wild type, an N_{FRET} value of 25.09 ± 0.95 (mean value ± S.E.) was measured. With CFP-rOct1(rOat1-l)/YFP-rOct1(rOat1-l), an N_{FRET} value of 17.40 ± 0.96 was obtained, and with CFP-rOct1(6ΔC-l)/YFP-rOct1(6ΔC-l), an N_{FRET} value of 5.41 ± 0.79 was obtained (Fig. 7). The differences between these values were highly significant ($p < 0.001$). To validate the FRET data, we also performed coexpression of a membrane-bound form of YFP (25) with CFP-rOct1 wild type. The obtained N_{FRET} value of 5.87 ± 0.67 was similar to the value obtained with CFP-rOct1(6ΔC-l)/YFP-rOct1(6ΔC-l) (5.41 ± 0.79), indicating that rOct1(6ΔC-l) does not form oligomers. It is noteworthy that the results obtained by FRET measurements *in vivo* are similar to the data obtained with solubilized transporters in the presence of LMPG showing strong oligomerization of rOct1 wild type, less complete oligomerization of rOct1(rOat1-l) (FRET, 69% of rOct1 wild type; *in vitro*, 65% of rOct1 wild type), and no significant oligomerization of rOct1(6ΔC-l) (FRET, 22% of rOct1 wild type; *in vitro*, 23% of rOct1 wild type). The data support the validity and *in vivo* relevance of our *in vitro* oligomerization assay by precipitation.

We also investigated whether 10 mM DTT is able to decrease the oligomerization of rOct1 wild type after expression in HEK293 cells. After coexpression of CFP-rOct1 wild type/YFP-rOct1 wild type, we determined a N_{FRET} value of 30.73 ± 1.38 in this experimental series (Fig. 8). When we incubated the cells for 5 s with 10 mM DTT, the N_{FRET} value decreased significantly to 22.21 ± 1.38 . After a 6-min incubation with 10 mM DTT, the N_{FRET} value decreased further to 16.07 ± 1.05 (Fig. 8). These data indicate that the equilibrium between monomers and dimers or oligomers within the plasma membrane is dependent on the integrity of extracellular disulfide bonds localized within the large extracellular loop.

Effect of DTT Treatment of rOct1 Wild Type Expressed in HEK293 Cells on Transport—To determine whether the DTT treatment of rOct1 expressed in HEK293 cells has an effect on transport properties of rOct1, we incubated these cells for 6 min with 10 mM DTT, washed the cells with 0.1 mM DTT to prevent reoxidation, and measured the concentration dependence of MPP⁺ uptake in the presence of 0.1 mM DTT (Fig. 9). Control measurements that were performed in the absence of DTT or in the presence of 0.1 mM DTT revealed similar maximal transport velocities per mg of cell protein (data not shown) and significantly higher Michaelis-Menten constant K_m values compared with cells treated with 10 mM DTT, K_m values in μM: (absence of DTT, 4.65 ± 0.75 ($n = 4$); 0.1 mM DTT, 4.55 ± 1.29 ($n = 3$); 10 mM DTT, 1.82 ± 0.45 ($n = 3$); $p < 0.01$, absence of DTT versus 10 mM DTT; $p < 0.01$, 0.1 mM DTT versus 10 mM DTT).

Demonstration That rOct1 Monomers within a rOct1 Tandem Protein Operate Independently—To determine whether rOct1 monomers within oligomers operate independently, we generated tandem proteins of rOct1 in which one or both rOct1 monomers could be blocked by covalent modification. In tandem proteins, the cytoplasmic N termini (21 amino acids long)

TABLE 2

Comparison of functional characteristics between rOct1 wild type, the oligomerizing loop mutant rOct1(rOat1-l), and the non-oligomerizing mutant rOct1(6ΔC-l) after reconstitution in proteoliposomes

The transporters were synthesized by cell-free expression, solubilized, purified, and reconstituted into proteoliposomes. Quinine-inhibitable uptake of [³H]MPP⁺ was measured in the presence of various concentrations of non-radioactive MPP⁺, and the apparent K_m values were determined by fitting the Michaelis-Menten equation to the data. Inhibition of [³H]MPP⁺ uptake by various concentrations of TEA⁺, TBuA⁺, or TPeA⁺ was measured, and the IC₅₀ values were determined by fitting the Hill equation to the data. Mean values ± S.D. of three experiments are indicated.

	MPP ⁺ uptake turnover <i>s</i> ⁻¹	MPP ⁺ uptake K_m μM	Inhibition of MPP ⁺ uptake IC ₅₀		
			TEA ⁺	TBuA ⁺ μM	TPeA ⁺
rOct1	19.5 ± 1.0	35.3 ± 1.5	150 ± 8.2	18.4 ± 0.31	2.84 ± 0.31
rOct1(Oat1-l)	8.2 ± 0.2 ^a	108 ± 9.3 ^b	173 ± 7.8 ^c	25.6 ± 2.1 ^b	3.63 ± 0.38
Oct1(6ΔC-l)	9.1 ± 0.3 ^a	105 ± 27 ^b	178 ± 10 ^c	27.2 ± 2.1 ^b	3.70 ± 0.47

^a $p < 0.001$ for difference to rOct1.

^b $p < 0.01$ for difference to rOct1.

^c $p < 0.05$ for difference to rOct1.

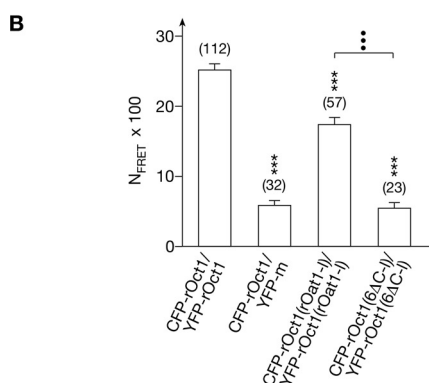
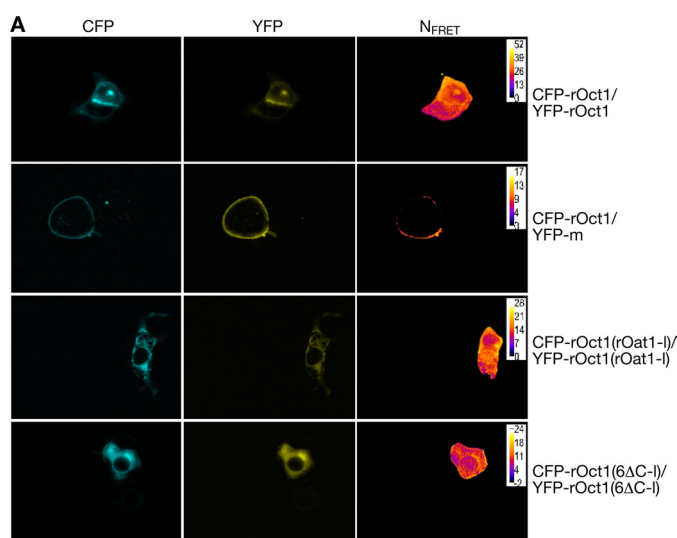


FIGURE 7. Oligomerization of rOct1, rOct1(rOat1-l), and rOct1(6ΔC-l) as demonstrated by FRET microscopy in intact cells. A, FRET images. HEK 293 cells were transiently transfected with cDNAs encoding CFP- and YFP-tagged rOct1, CFP-tagged rOct1, and membrane-associated YFP (*m*-YFP), CFP- and YFP-tagged rOct1(rOat1-l), and CFP- and YFP-tagged rOct1(6ΔC-l). Two days after transfection, epifluorescence microscopy was performed. The first and second columns show images obtained with CFP and YFP filter sets; the third column displays a corrected and normalized FRET image (N_{FRET}) established with PIX-FRET. The color code is presented in the last column. In all images, background fluorescence was subtracted. The indicated images are representative of 4–8 experiments. B, normalized FRET efficiencies (N_{FRET} values). Mean ± S.E. (error bars) values are indicated. The numbers of measured cells are given in parentheses. ***, $p < 0.001$, difference from rOct1-w; ●●●, $p < 0.001$. The data indicate that the large extracellular loop is pivotal for oligomerization.

were linked to the cytoplasmic C termini (42 amino acids long) to force dimerization of the connected tandem proteins. To avoid nonspecific reactions with an SH group reagent

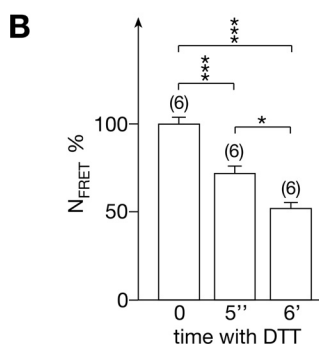
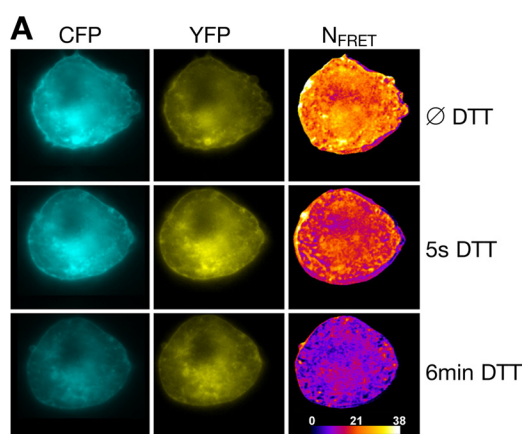


FIGURE 8. Oligomerization of rOct1 expressed in HEK293 cells is destroyed after incubation with DTT. A, FRET images. HEK 293 cells were transiently transfected with cDNAs encoding CFP- and YFP-tagged rOct1. Two days after transfection, epifluorescence microscopy was performed without DTT incubation, after incubation for 5 s with 10 mM DTT, and after incubation for 6 min with 10 mM DTT. The first and second column show images obtained with CFP and YFP filter sets, whereas the third column displays a corrected and normalized FRET image (N_{FRET}). Representative images with subtracted background fluorescence are shown. B, normalized FRET efficiencies (N_{FRET} values). Mean ± S.E. (error bars) values are indicated. The numbers of measured cells are given in parentheses. *, $p < 0.05$; **, $p < 0.01$; ***, $p < 0.001$. The experiment suggests that reduction of disulfide bridges within the large extracellular loop rapidly alters the equilibrium between rOct1 monomers and oligomers in the plasma membrane.

employed to inhibit modified rOct1 transporter, in all rOct1 mutants, 10 cysteine residues were replaced by serine, alanine, or methionine rOct1(10ΔC) (17). When rOct1(10ΔC) or rOct1(10ΔC)-rOct1(10ΔC) tandem protein was expressed in oocytes of *X. laevis* by injecting identical amounts of transporter cRNAs, the uptake rate of 9 μM TEA⁺ expressed by the tandem protein amounted to 50.6 ± 13.3% of that obtained

Oligomerization of Organic Cation Transporter 1

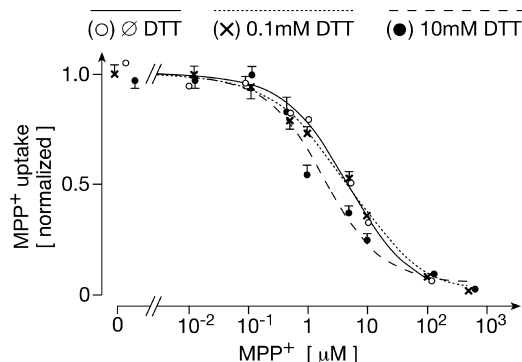


FIGURE 9. Incubation of rOct1 expressed in HEK293 cells with DTT alters transport kinetics. Cells were preincubated for 6 min with PBS containing 10 mM DTT, washed with PBS containing 0.1 mM DTT, and incubated for 10 min in the same buffer (●). Control cells were preincubated, washed, and incubated with PBS (○) or PBS containing 0.1 mM DTT (×). Substrate concentration dependence of MPP⁺ uptake into HEK293 cells stably transfected with rOct1 was measured in the absence of DTT (○) or in the presence of 0.1 mM DTT (×, ●). Mean values ± S.D. (error bars) of 12–16 measurements from three or four experiments are presented. The uptake rates of the individual measurements are normalized. The Hill equation is fitted to the data.

with rOct1(10ΔC) ($n = 30$ each). In some mutants, glycine in position 478 was replaced by cysteine (rOct1(10ΔC,G478C)) to introduce sensitivity to the transported SH group reagent (MTSET).³ When oocytes expressing rOct1(10ΔC,G478C) were incubated for 10 min with 100 μM MTSET, 73% of TEA⁺ uptake activity was blocked irreversibly, whereas uptake was not changed in oocytes expressing rOct1(10ΔC) (Fig. 10A). Similarly, in oocytes expressing tandem protein rOct1(10ΔC-G478C)-rOct1(10ΔC-G478C), 85% of expressed TEA⁺ uptake was irreversibly blocked after a 10-min incubation with 100 μM MTSET, whereas MTSET did not change TEA⁺ transport expressed by tandem protein rOct1(10ΔC)-rOct1(10ΔC) (Fig. 10A). When oocytes expressing tandem protein rOct1(10ΔC)-rOct1(10ΔC-G478C) were incubated for 10 min with 100 μM MTSET, 28% of expressed TEA⁺ transport was blocked. This suggests that blockage of one monomer in the tandem protein did not change uptake of 9 μM TEA⁺ mediated by the other monomer. To determine whether affinities of organic cation substrates and inhibitors are influenced by dimerization, we measured the apparent K_m values for TEA⁺ and MPP⁺ uptake in oocytes expressing rOct1(10ΔC)-rOct1(10ΔC,G478C) tandem proteins without and with blockage of one monomer by treatment with MTSET. Without and with MTSET treatment, about the same K_m values were obtained (TEA⁺ without MTSET, 94 ± 14.6 μM; TEA⁺ with MTSET, 101 ± 13.2 μM; MPP⁺ without MTSET, 7.7 ± 1.3 μM; MPP⁺ with MTSET, 7.3 ± 1.2 μM) (Fig. 10B). Similarly, the same IC₅₀ values for inhibition of MPP⁺ (0.1 nM) uptake by TBuA⁺ were obtained without and with MTSET treatment (1.53 ± 0.20 versus 1.49 ± 0.19 μM, three independent experiments). The data strongly suggest that the substrate affinity of rOct1 is not changed by oligomerization.

DISCUSSION

This paper shows that the tertiary structure of the large extracellular loop of rOct1, which is stabilized by disulfide

³ B. Egenberger, V. Gorboulev, N. Gottlieb, T. Keller, D. Gorbunov, T. Müller, and H. Koepsell, unpublished data.

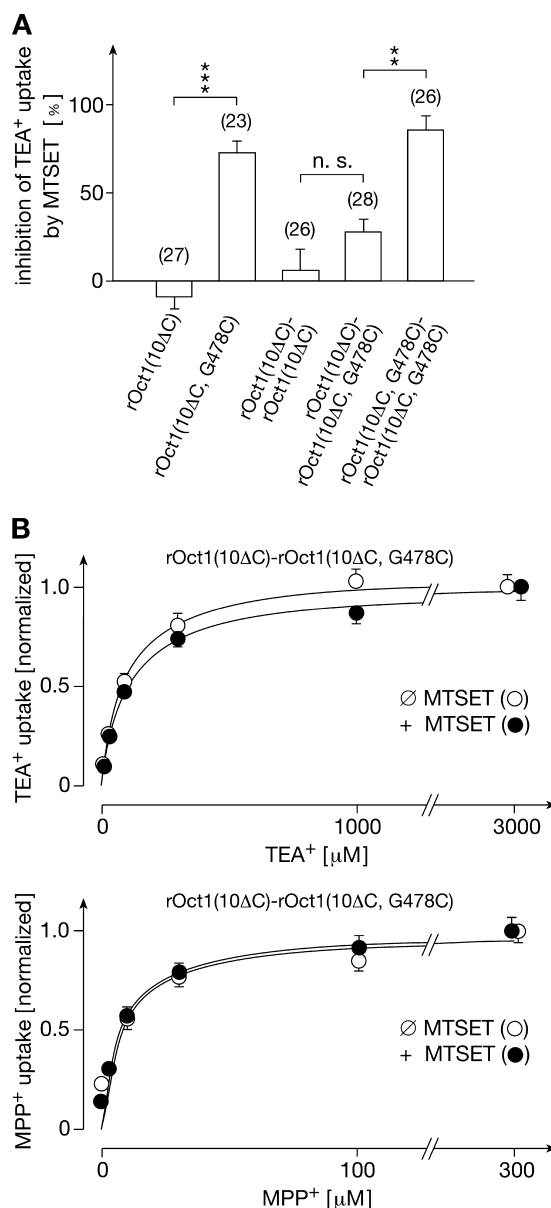


FIGURE 10. Both rOct1 monomers in a rOct1 tandem dimer are functionally active and transport independently. A, the covalently binding substrate analog MTSET blocks monomers in a rOct1 tandem protein, which contains a cysteine residue in position 478. Oocytes were injected with cRNAs encoding rOct1(10ΔC), rOct1(10ΔC) in which Gly-478 was replaced by cysteine rOct1(10ΔC,G478C), and the indicated tandem dimer proteins. After 3 days of incubation for expression, the cRNA-injected oocytes and non-injected control oocytes were incubated for 10 min in the absence or presence of 100 μM MTSET. After washing, TEA⁺ uptake was measured after 15 min of incubation with 9 μM [¹⁴C]TEA⁺. Uptake rates of cRNA-injected oocytes were corrected for uptake in non-injected control oocytes. Mean values ± S.E. (error bars) that were derived from three independent different experiments are indicated. The numbers of measured oocytes are indicated in parentheses. **, $p < 0.01$; ***, $p < 0.001$. B, concentration dependence of TEA⁺ and MPP⁺ uptake into oocytes expressing tandem protein rOct1(10ΔC)-rOct1(10ΔC,G478C) without and with pretreatment with MTSET. Oocytes were incubated for 10 min in the absence of MTSET or with 100 μM MTSET. Cells were washed, and uptake of [¹⁴C]TEA⁺ or [³H]MPP⁺ was measured in the presence of various concentrations of nonradioactive TEA⁺ or MPP⁺, respectively. Uptake in non-injected oocytes was subtracted. Mean values ± S.E. of 26–30 oocytes from three independent experiments are indicated. The data show that both monomers within the rOct1 tandem protein are capable of transporting organic cations and that the affinity for transport of TEA⁺ or MPP⁺ transport by one monomer is not altered when transport function of the other monomer is blocked.

bonds, is required for oligomerization and membrane insertion of rOct1 and has an effect on the affinity of organic cations independently of the oligomerization. Evidence is presented which indicates that the rOct1 monomers of the oligomeric complex transport their substrates independently. The results are required for the elucidation of the functional mechanism of organic cation transporters and to understanding how polymorphisms in the large extracellular loop may change function.

Oligomerization of rOct1 was investigated in solution in the presence of detergents and *in vivo* after transient expression of rOct1 in HEK293 cells. Because the structural integrity of the large extracellular loop of rOct1 and/or intracellular oligomerization appears essential for effective plasma membrane location of rOct1, and HEK293 cells express some endogenous transport activity of MPP⁺ and TEA⁺, functional characterization of non-oligomerizing rOct1 mutants in HEK293 cells was not possible. At variance, functional activity of loop mutants could be characterized by expression in oocytes of *X. laevis* in which the background activity of endogenous TEA⁺ and MPP⁺ uptake is very low. In HEK293 cells, we were able to investigate oligomerization of loop mutants labeled with CFP and YFP that were transiently expressed in these cells because these measurements are not influenced by endogenous transporters and highly expressing cells could be selected for analysis. We observed that oligomerization of solubilized rOct1 is dependent on detergents. However, because our results obtained by coprecipitation of rOct1 proteins in the presence of 1% LMPG and 0.5% CHAPS were very similar to the results obtained by FRET measurements in HEK293 cells, our coprecipitation experiments provide a reliable model for the *in vivo* situation.

When the six cysteine residues in the large extracellular loop of rOct1 were replaced by serines or when the disulfide bridge(s) in the loop were reduced by DTT, oligomerization was abolished. The oligomerization is reversible because covalent dimerization of rOct1 via intermolecular disulfide bridges could be excluded, and 5-s incubation of HEK293 cells expressing rOct1 with 10 mM DTT decreased the amount of rOct1 oligomers. Using the precipitation assay, we observed that oligomerization can also be mediated by the large extracellular loop of rOat1; however, the large loops of rOct1 and rOat1 do not mediate hetero-oligomerization. Oligomerization was found between rOat1 and the rOct1 chimeras containing the large extracellular loop of rOat1 (rOct1(rOat1-l)) but not between rOct1(rOat1-l) and rOct1. We cannot exclude the possibility that rOct1 contains an additional contact region in its sixth TMH in analogy to hOAT1 (13); however, this potential contact region is apparently not sufficient for oligomerization because no oligomerization was observed between rOct1 and rOct1(rOat1-l).

Trying to answer the important question of whether oligomerization of rOct1 has an effect on the functional characteristics of organic cation transport, we compared functional properties between rOct1 wild type, the oligomerizing loop mutant rOct1(rOat1-l), and the non-oligomerizing loop mutant rOct1(6ΔCys). For comparison, we measured MPP⁺ uptake after expression of rOct1 and rOct1 mutants in oocytes, measured MPP⁺ binding to purified proteins that had been precipitated, and measured MPP⁺ transport into proteolipo-

somes. Similar results were obtained with the different assays showing that the functional properties of both loop mutants were similar but in most cases significantly different from rOct1 wild type. The K_m values for MPP⁺ uptake of both loop mutants expressed in oocytes were similar but higher compared with rOct1 wild type. Consistently, the K_D values for MPP⁺ binding to both precipitated loop mutants were similar and higher (50%) compared with wild type rOct1. Also, in proteoliposomes, the K_m values for MPP⁺ uptake by rOct1(rOat1-l) and rOct1(6ΔC-l) were similar and higher (300%) compared with MPP⁺ uptake by rOct1 wild type. In proteoliposomes, we obtained virtually the same K_i values for inhibition of MPP⁺ uptake via both loop mutants by TEA⁺, TBuA⁺, or TPeA⁺. The K_i values of the loop mutants for TEA⁺ and TBuA⁺ were slightly but significantly higher compared with rOct1 wild type, whereas the K_i values for inhibition of MPP⁺ uptake by TPeA⁺ were identical. The data indicate that the structure of the large extracellular loop influences the affinity of rOct1 for organic cation binding but that transport is independent of oligomerization. The observation that the transport characteristics of the non-oligomerizing loop mutant rOct1(6ΔC-l) were virtually identical to those of the oligomerizing loop mutant rOct1(rOat1-l) strongly suggests that the function of rOct1 is not dependent on oligomerization. The finding that the K_m value for MPP⁺ uptake was decreased when the disulfide bridge(s) in the large extracellular loop were disrupted by DTT treatment, leading to a decrease of oligomerization, does not contradict this interpretation because disruption of disulfide bond(s) leads to a structural change that may increase MPP⁺ affinity independent of oligomerization.

Our data showing that the mutations within the large extracellular loops of OCTs not only decrease the amount of transporter molecules within the plasma membrane but may also affect substrate affinity have biomedical impact. Frequent non-synonymous polymorphisms have been observed in the large extracellular loop of human OCT1 (3), and uptake of metformin into hepatocytes by hOCT1 is important for antidiabetic function (36). Antibodies, lectins, or reducing agents in the blood that interact with the glycosylated extracellular loop of hOCT1 may also decrease substrate affinity. The question of how mutations in the large extracellular loop can change substrate affinity may be answered as follows. We consider it improbable that the large extracellular loop participates directly in substrate binding. For this purpose, it had to dip deeply into the outward open cleft and had to be retracted when the transporter switched from the outward-open to the inward-open conformation during substrate translocation. Most probably, the large extracellular loop that connects TMH1 and TMH2 exhibits an indirect effect on the cation binding region. For example, the structure of the loop may influence the positioning of TMH2, which participates directly in substrate binding and interacts with TMH4 that is also directly involved in substrate binding (9). Note that replacement of Phe-160 in TMH2 by alanine increased the affinity for extracellular corticosterone and TBuA⁺ (37), whereas exchange of tryptophan 218 by tyrosine in TMH4 increased the affinity for TEA⁺ and MPP⁺ (7).

Oligomerization of Organic Cation Transporter 1

To determine whether both rOct1 monomers within an rOct1 dimer are functionally active and whether they operate independently or in a cooperative fashion, we synthesized rOct1 tandem proteins in which one monomer or both monomers could be blocked covalently. We linked the rOct1 monomers via their long intracellular N and C termini to allow undisturbed dimerization, similar to the *in vivo* situation. Rapid covalent blockage of the transport function was achieved by introducing a cysteine residue in TMH11 at position 478, which is located one α -helix turn above aspartate 475, which is directly involved in TEA⁺ binding. For these experiments, rOct1 mutants were used in which all endogenous cysteine residues except those in the large extracellular loop had been replaced. Without and with blockage of one rOct1 monomer in the rOct1 tandem protein, we obtained about the same K_m values for uptake of TEA⁺ or MPP⁺. This observation strongly suggests that both monomers operate independently without exhibiting significant cooperative effects. This interpretation is supported by the fact that the substrate dependence for OCT-mediated uptake of organic cations could always be fitted by the Michaelis-Menten equation, showing no indication of cooperativity (9).

The observation that rOct1 monomers operate independently in the oligomer complex has important theoretical implications. Interpreting previous data on mutagenesis in combination with homology modeling of rOct1, we assumed independent monomeric function of rOct1 for simplicity (9). The present data provide a *post hoc* justification for this assumption. Assuming monomeric function of rOct1, well supported hypotheses concerning substrate binding and translocation have been raised. Neglecting allosteric effects of substrate binding to different monomers, differential effects of single point mutations on different substrates were interpreted to indicate that the substrate binding region of rOct1 contains overlapping binding domains for different substrates (10, 37). Although our present data do not exclude subtle allosteric effects between monomers, they show that allosteric interaction between monomers does not have main functional importance. In conclusion, we have provided evidence that the large extracellular loop of organic cation transporters and organic anion transporters is pivotal for oligomerization, is critical for membrane targeting, and influences substrate affinity.

Acknowledgments—We thank Ursula Roth for expert and engaged technical assistance and Michael Christof for preparing the figures.

REFERENCES

1. Koepsell, H., Lips, K., and Volk, C. (2007) *Pharm. Res.* **24**, 1227–1251
2. Rizwan, A. N., and Burckhardt, G. (2007) *Pharm. Res.* **24**, 450–470
3. Nies, A. T., Koepsell, H., Damme, K., and Schwab, M. (2011) *Handb. Exp. Pharmacol.* **201**, 105–167
4. Gründemann, D., Gorboulev, V., Gambaryan, S., Veyhl, M., and Koepsell, H. (1994) *Nature* **372**, 549–552
5. Sweet, D. H., Wolff, N. A., and Pritchard, J. B. (1997) *J. Biol. Chem.* **272**, 30088–30095
6. Ciarimboli, G., and Schlatter, E. (2005) *Pflugers Arch.* **449**, 423–441
7. Popp, C., Gorboulev, V., Müller, T. D., Gorbunov, D., Shatskaya, N., and Koepsell, H. (2005) *Mol. Pharmacol.* **67**, 1600–1611
8. Perry, J. L., Dembla-Rajpal, N., Hall, L. A., and Pritchard, J. B. (2006) *J. Biol. Chem.* **281**, 38071–38079
9. Koepsell, H. (2011) *Biol. Chem.* **392**, 95–101
10. Gorbunov, D., Gorboulev, V., Shatskaya, N., Mueller, T., Bamberg, E., Friedrich, T., and Koepsell, H. (2008) *Mol. Pharmacol.* **73**, 50–61
11. Hong, M., Xu, W., Yoshida, T., Tanaka, K., Wolff, D. J., Zhou, F., Inouye, M., and You, G. (2005) *J. Biol. Chem.* **280**, 32285–32290
12. Keller, T., Schwarz, D., Bernhard, F., Dötsch, V., Hunte, C., Gorboulev, V., and Koepsell, H. (2008) *Biochemistry* **47**, 4552–4564
13. Duan, P., Li, S., and You, G. (2011) *Mol. Pharmacol.* **79**, 569–574
14. Keller, T., Elfeber, M., Gorboulev, V., Reiländer, H., and Koepsell, H. (2005) *Biochemistry* **44**, 12253–12263
15. Gorboulev, V., Volk, C., Arndt, P., Akhoundova, A., and Koepsell, H. (1999) *Mol. Pharmacol.* **56**, 1254–1261
16. Gorboulev, V., Shatskaya, N., Volk, C., and Koepsell, H. (2005) *Mol. Pharmacol.* **67**, 1612–1619
17. Sturm, A., Gorboulev, V., Gorbunov, D., Keller, T., Volk, C., Schmitt, B. M., Schlachtbauer, P., Ciarimboli, G., and Koepsell, H. (2007) *Am. J. Physiol. Renal Physiol.* **293**, F767–F779
18. Ho, S. N., Hunt, H. D., Horton, R. M., Pullen, J. K., and Pease, L. R. (1989) *Gene* **77**, 51–59
19. Klamm, C., Löhr, F., Schäfer, B., Haase, W., Dötsch, V., Rüterjans, H., Glaubitz, C., and Bernhard, F. (2004) *Eur. J. Biochem.* **271**, 568–580
20. Valentin, M., Kühnkamp, T., Wagner, K., Krohne, G., Arndt, P., Baumgarten, K., Weber, W., Segal, A., Veyhl, M., and Koepsell, H. (2000) *Biochim. Biophys. Acta* **1468**, 367–380
21. Schmid, J. A., and Sitte, H. H. (2003) *Curr. Opin. Oncol.* **15**, 55–64
22. Bartholomäus, I., Milan-Lobo, L., Nicke, A., Dutertre, S., Hastrup, H., Jha, A., Gether, U., Sitte, H. H., Betz, H., and Eulenburg, V. (2008) *J. Biol. Chem.* **283**, 10978–10991
23. Susic, S., Dallinger, S., Zdrzil, B., Weissensteiner, R., Jørgensen, T. N., Holy, M., Kudlacek, O., Seidel, S., Cha, J. H., Gether, U., Newman, A. H., Ecker, G. F., Freissmuth, M., and Sitte, H. H. (2010) *J. Biol. Chem.* **285**, 10924–10938
24. Feige, J. N., Sage, D., Wahli, W., Desvergne, B., and Gelman, L. (2005) *Microsc. Res. Tech.* **68**, 51–58
25. Hein, P., Frank, M., Hoffmann, C., Lohse, M. J., and Bünemann, M. (2005) *EMBO J.* **24**, 4106–4114
26. Busch, A. E., Quester, S., Ulzheimer, J. C., Gorboulev, V., Akhoundova, A., Waldegger, S., Lang, F., and Koepsell, H. (1996) *FEBS Lett.* **395**, 153–156
27. Veyhl, M., Spangenberg, J., Püschel, B., Poppe, R., Dekel, C., Fritzsche, G., Haase, W., and Koepsell, H. (1993) *J. Biol. Chem.* **268**, 25041–25053
28. Veyhl, M., Wagner, C. A., Gorboulev, V., Schmitt, B. M., Lang, F., and Koepsell, H. (2003) *J. Membr. Biol.* **196**, 71–81
29. Gründemann, D., and Koepsell, H. (1994) *Anal. Biochem.* **216**, 459–461
30. Arndt, P., Volk, C., Gorboulev, V., Budiman, T., Popp, C., Ulzheimer-Teuber, I., Akhoundova, A., Koppatz, S., Bamberg, E., Nagel, G., and Koepsell, H. (2001) *Am. J. Physiol. Renal Physiol.* **281**, F454–F468
31. Kamsteeg, E. J., and Deen, P. M. (2001) *Biochem. Biophys. Res. Commun.* **282**, 683–690
32. Farhan, H., Freissmuth, M., and Sitte, H. H. (2006) *Handb. Exp. Pharmacol.* **175**, 233–249
33. Kilic, F., and Rudnick, G. (2000) *Proc. Natl. Acad. Sci. U.S.A.* **97**, 3106–3111
34. Brosig, B., and Langosch, D. (1998) *Protein Sci.* **7**, 1052–1056
35. Xia, Z., and Liu, Y. (2001) *Biophys. J.* **81**, 2395–2402
36. Shu, Y., Sheardown, S. A., Brown, C., Owen, R. P., Zhang, S., Castro, R. A., Ianculescu, A. G., Yue, L., Lo, J. C., Burchard, E. G., Brett, C. M., and Giacomini, K. M. (2007) *J. Clin. Invest.* **117**, 1422–1431
37. Volk, C., Gorboulev, V., Kotsch, A., Müller, T. D., and Koepsell, H. (2009) *Mol. Pharmacol.* **76**, 275–289